

Thermal transport in graphene nanoribbons supported on SiO₂

Z. Aksamija* and I. Knezevic†

Department of Electrical and Computer Engineering, University of Wisconsin-Madison, Madison, Wisconsin 53706, USA

(Received 29 July 2012; published 15 October 2012)

We present a theoretical model for thermal transport in graphene nanoribbons (GNRs) on SiO₂ based on solving the phonon Boltzmann transport equation. Thermal transport in supported GNRs is characterized by a complex interplay between line edge roughness (LER) and internal scattering, as captured through an effective LER scattering rate that depends not only on the surface roughness features, but also on the strength of internal scattering mechanisms (substrate, isotope, and umklapp phonon scattering). Substrate scattering is the dominant internal mechanism, with a mean free path (mfp) of approximately 67 nm. In narrow supported GNRs ($W < 130$ nm, i.e., roughly twice the mfp due to substrate scattering), phonon transport is limited by LER and spatially anisotropic. For intermediate widths ($130 \text{ nm} < W < 1 \mu\text{m}$) a competition between LER and substrate scattering governs transport, while thermal transport in wide GNRs ($W > 1 \mu\text{m}$) is dominated by substrate scattering and spatially isotropic. Thermal transport in supported GNRs can be tailored by controlling the ribbon width and edge roughness. We conclude that narrow ribbons act as longitudinal heat conduits while wide ribbons act as good omnidirectional heat spreaders.

DOI: [10.1103/PhysRevB.86.165426](https://doi.org/10.1103/PhysRevB.86.165426)

PACS number(s): 63.22.Rc, 63.20.K-, 63.22.-m, 63.70.+h

I. INTRODUCTION

Graphene possesses superior thermal conductivity^{1,2} important for the potential applications of graphene-based nanostructures as devices and heat spreaders in dense microelectronic circuits.² Experimental work on the thermal properties of graphene spurred a number of theoretical studies.³ Calculations based on the relaxation-time approximation (RTA),⁴⁻⁶ tight-binding,⁷ molecular dynamics,^{8,9} and the ballistic approximation¹⁰ confirmed graphene's excellent thermal properties. However, device applications of graphene typically employ samples supported on SiO₂,¹¹ where the interaction between graphene and the substrate surface variations drastically reduce graphene's thermal conductivity relative to its suspended counterpart.¹²

Graphene nanoribbons (GNRs), narrow strips of graphene, are important for a number of applications. Logic devices have to be made from very narrow GNRs in order to lithographically tune the band gap and achieve the required on-off ratios.^{13,14} In high-frequency applications, it was found that devices based on wide GNRs benefit from lateral heat spreading and dissipate efficiently into the substrate,¹¹ while those made from narrow ribbons mainly dissipate heat longitudinally, into the metallic contacts.¹⁵ These experimental findings raise questions about the parallel and cross-ribbon components of the thermal conductivity tensor in supported GNR devices.

In narrow GNRs, line edge roughness (LER) has been shown to reduce the lattice thermal conductivity relative to its value in large flakes.^{7-9,16} Moreover, when graphene is cut into nanoribbons, directional anisotropy of thermal conductivity appears,¹⁶⁻¹⁸ in contrast to the isotropic ballistic thermal conductivity of graphene.¹⁹ Despite tremendous experimental and theoretical progress, a study treating both substrate and line edge roughness effects on thermal transport, as well as their mutual interplay and the resulting directional anisotropy of the lattice thermal conductivity tensor, is lacking.

In this paper, we explore lattice thermal transport in GNRs supported on a SiO₂ substrate. We demonstrate the sensitivity

of the lattice thermal conductivity in GNRs to the edge properties, based on solving the phonon Boltzmann transport equation (pBTE) under the relaxation time approximation. We derive a solution to the pBTE in the cross-ribbon direction with partially diffuse edges in the presence of competing substrate roughness, umklapp phonon, and isotope scattering processes. Based on this solution, we compute the lattice thermal conductivity tensor and show that it has distinct components along and across the ribbon. The parallel/cross-ribbon anisotropy increases with decreasing width and increasing line edge roughness, and with decreasing temperature. In supported nanoribbons, we identify three ranges of the GNR width W based of the competition between edge roughness and substrate scattering: (1) *narrow ribbons* ($W < 130$ nm, 130 nm roughly being twice the length of the substrate-limited mean free path), where line-edge roughness dominates and directional anisotropy in phonon transport is pronounced, (2) *medium-width ribbons* ($130 \text{ nm} < W < 1 \mu\text{m}$), where substrate and roughness scattering compete and the two edges are effectively decoupled, and (3) *wide ribbons* ($W > 1 \mu\text{m}$), where substrate scattering dominates and thermal transport is isotropic. We conclude that thermal conductivity of narrow GNRs can be tailored by controlling their width and edge properties. Coupled with good electronic transport properties, this opens up the possibility of using GNRs for high-efficiency thermoelectric conversion.

The paper is organized as follows: In Sec. II, we present the phonon transport model and derive the solution of the steady-state phonon Boltzmann transport equation in the presence of competing effects of roughness scattering at the edges of the ribbon and other scattering mechanisms, including substrate, isotope, and umklapp phonon, within the ribbon. In Sec. III, we present the parallel (along the ribbon) and perpendicular (laterally across the ribbon) components of the thermal conductivity tensor in narrow graphene nanoribbons. We compare our results to available experimental data and discuss the interplay between the line edge roughness and substrate scattering, as well as their combined effect on thermal

conductivity. We conclude in Sec. IV, with a brief summary and a few final remarks.

II. PHONON TRANSPORT MODEL

Phonons are the dominant carriers of heat in graphene.¹² We model lattice thermal transport in GNRs by solving pBTE. Due to the absence of the Casimir limit in GNRs,²⁰ we cannot treat edge roughness scattering separately from the other scattering mechanisms; instead, the complete pBTE must be solved, taking into account all the scattering mechanisms occurring within the ribbon, in addition to the diffusive interactions of phonons with the rough edges. We are interested in the linear response of the phonon population to small perturbations, such as the application of a small uniform temperature gradient. Since the dominant edge and substrate scattering processes are both elastic, the single-mode relaxation time approximation (RTA) form of the pBTE can be used, and the pBTE can be written in the steady state as

$$\vec{v}_{\vec{q}} \cdot \nabla N_{\vec{q}}(x, y) = -\frac{N_{\vec{q}}(x, y) - N_{\vec{q}}^0(T)}{\tau_{\text{int.}}(\vec{q})}, \quad (1)$$

where $N_{\vec{q}}^0(T)$ is the equilibrium Bose-Einstein phonon distribution, $N_{\vec{q}}(x, y)$ is the number of phonons with wave vector \vec{q} at spatial position (x, y) in the ribbon (the branch phonon index is omitted for brevity), and $\vec{v}_{\vec{q}}$ is the mode velocity. The total ‘‘internal’’ relaxation rate, $\tau_{\text{int.}}^{-1}(\vec{q})$, is a sum of the scattering rates due to all the mechanisms that take place within the ribbon except line edge roughness scattering, which includes umklapp phonon-phonon, isotope, impurity, as well as substrate interactions. The expressions for the umklapp phonon-phonon and isotope scattering rates were taken from Ref. 16. Substrate scattering is modeled as a point interaction with small patches where the ribbon is in contact with the substrate.¹² This model leads to a phonon lifetime that is proportional to the vibrational density of states (vDOS) $\rho(\omega)$ and the form factor $\phi(\vec{q})$ of the contact patches, assumed to be circular in shape:

$$\tau_{\text{sub.}}^{-1}(\vec{q}) = \frac{\pi}{2} \frac{N_{\text{scat.}}}{N_c \omega^2(\vec{q})} \phi(\vec{q}) \left(\frac{K_f}{M_C} \right)^2 \rho(\omega), \quad (2)$$

where $N_{\text{scat.}}$ is the density of scattering centers, N_c is the number of contact atoms in the contact patch, M_C is the mass of a carbon atom, and $K_f = 0.7 \text{ Nm}^{-1}$ is the interaction force between graphene and the substrate, following Seol *et al.*¹² The substrate scattering model assumes that the contact between the graphene and the substrate is through circular patches of a single effective, or average, size. This assumption limits the model to substrates that have relatively uniform atomic-scale surface roughness, such as SiO₂ used in the present study. Other substrates with larger surface variation could lead to contact patches with more pronounced variations in size and shape, which could be addressed in future work by using a spatially varying substrate scattering rate to match the shapes and positions of the interaction patches between the graphene and the substrate.

We consider the response of the phonon population to the application of a small uniform temperature gradient. The solution to the pBTE in the absence of boundaries has the

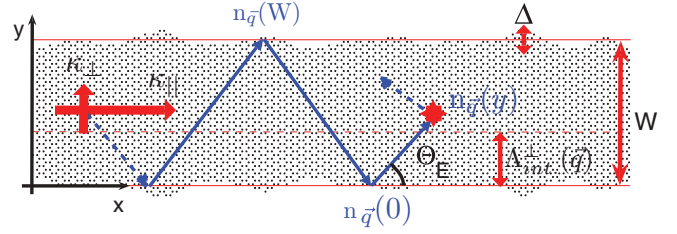


FIG. 1. (Color online) Schematic representation of a graphene nanoribbon, showing the ribbon width W , line edge rms roughness Δ , and a phonon path through the ribbon with the pBTE solution $n_{\vec{q}}(y)$ and boundary conditions $n_{\vec{q}}(W)$ and $n_{\vec{q}}(0)$ marked along that path. The phonon path inside the ribbon is interrupted by an internal scattering event. Thermal conductivities in the parallel (κ_{\parallel}) and perpendicular (κ_{\perp}) directions are also depicted.

familiar homogeneous ‘‘bulk’’ RTA form where the response is proportional to the perturbing temperature gradient

$$R_{\vec{q}} = \tau_{\text{int.}}(\vec{q}) \vec{v}_{\vec{q}} \cdot \nabla T [dN_{\vec{q}}^0(T)/dT]. \quad (3)$$

When boundaries are introduced, the solution becomes position-dependent along the y direction, normal to the edges of the ribbon. Therefore, we write the complete solution as $N_{\vec{q}}(x, y) = N_{\vec{q}}^0(T) + n_{\vec{q}}(y)$ and introduce it into the pBTE²¹ to obtain

$$\vec{v}_{\vec{q}} \cdot \nabla T \frac{dN_{\vec{q}}^0(T)}{dT} + v_{\vec{q}}^{\perp} \frac{\partial n_{\vec{q}}(y)}{\partial y} = \frac{n_{\vec{q}}(y)}{\tau_{\text{int.}}}. \quad (4)$$

For a phonon wave that leaves the bottom edge ($y = 0$) with a normal wave vector component along y ($q^{\perp} > 0$), the solution starts from $n_{\vec{q}}(0)$ (the boundary value at $y = 0$) and approaches the RTA value [Eq. (3)] away from the edge

$$n_{\vec{q}}^{\perp}(y) = R_{\vec{q}} - [R_{\vec{q}} - n_{\vec{q}}(0)] \exp[-y/\Lambda_{\text{int.}}^{\perp}(\vec{q})]. \quad (5)$$

Here, $\Lambda_{\text{int.}}(\vec{q}) = v_{\vec{q}} \tau_{\text{int.}}(\vec{q})$ is the mean free path (mfp) due to internal scattering and $\Lambda_{\text{int.}}^{\perp}(\vec{q})$ is its component corresponding to motion across the ribbon, perpendicular to its edges. The solution for a phonon leaving the opposite boundary at $y = W$ with a normal wave vector component in the negative y direction ($q^{\perp} < 0$), as depicted in Fig. 1, is

$$n_{\vec{q}}^{\perp}(y) = R_{\vec{q}} - [R_{\vec{q}} - n_{\vec{q}}(W)] \exp[-(W - y)/\Lambda_{\text{int.}}^{\perp}(\vec{q})].$$

At $y = 0$, the following boundary condition holds for partially specular reflection of the phonon wave^{22,23}

$$N_{\vec{q}}(0) = p(\vec{q}) N_{\vec{q}}(0) + [1 - p(\vec{q})] N_{\vec{q}}^0(T), \quad (6)$$

where \tilde{q} is a specular reflection of \vec{q} from an edge ($\tilde{q}_y = -q_y$). In this work, in order to accurately treat phonon scattering from rough edges with a given rms roughness height (Δ), we employ a *momentum-dependent* specularly parameter $p(\vec{q}) = \exp(-4q^2 \Delta^2 \sin^2 \Theta_E)$ ^{16,24} that represents the fraction of specular reflections to the total number of reflections from a rough boundary [$0 \leq p(\vec{q}) \leq 1$]. This expression allows us to connect the specularly parameter $p(\vec{q})$ directly to the rms magnitude of the surface roughness Δ , the phonon wave vector \vec{q} , and the angle Θ_E between the incident phonon wave vector and the edge direction.

Substituting $N_{\vec{q}}(0) = N_{\vec{q}}^0(T) + n_{\vec{q}}(0)$ into Eq. (6), we find the boundary condition on the spatially varying part of the

solution as $n_{\vec{q}}(0) = p(\vec{q})n_{\vec{q}}(0)$ at the bottom ($y = 0$) edge. An equivalent boundary condition is applied to the phonons moving in the negative y direction ($q^\perp < 0$) at the $y = W$ boundary for the $n_{\vec{q}}^-(y)$ solution. As an ideally smooth ribbon would be symmetric upon reflection from the $y = W/2$ plane, $n_{\vec{q}}(0) = n_{\vec{q}}(W)$, so $n_{\vec{q}}(0) = p(\vec{q})n_{\vec{q}}(W)$, which is then introduced into Eq. (5) to solve for $n_{\vec{q}}$. Finally,

$$n_{\vec{q}}^\pm(y) = R_{\vec{q}} \left\{ 1 - \frac{[1 - p(\vec{q})] \exp[-y/\Lambda_{\text{int}}^\perp(\vec{q})]}{1 - p(\vec{q}) \exp[-W/\Lambda_{\text{int}}^\perp(\vec{q})]} \right\}. \quad (7)$$

The solution $n_{\vec{q}}^-(y)$ for a phonon wave in the negative y direction ($q^\perp < 0$) would be analogous, only with $(W - y)$ replacing y due to inversion symmetry of the system. We note here that an identical solution is also obtained by tracing the solution through an infinite series of partially specular reflections and then summing the infinite series.²⁵

The spatially resolved solution to the pBTE enables us to take a close look at the role that edge scattering plays in phonon transport. At any point across the ribbon, the heat flux carried by the modes with $q^\perp > 0$ can then be given as a function of position y as

$$\vec{Q}^+(y) = \hbar \sum_{q^\perp > 0} \omega(\vec{q}) \vec{v}_{\vec{q}} n_{\vec{q}}^+(y), \quad (8)$$

and analogously for $\vec{Q}^-(y)$, which is given by a sum over all phonon modes with $q^\perp < 0$ (of course, the sum also subsumes the suppressed branch index). The heat flux vectors are functions of position because of the effect of edges captured by $n_{\vec{q}}^{+/-}(y)$ [Eq. (7)]. If we apply a thermal gradient in a certain direction, then the ratio of the heat flux in the same direction to the magnitude of the gradient, $|\nabla T|$, will yield the thermal conductivity in the direction of the gradient. Consequently, $\kappa^{+/-}(y) = |\vec{Q}^{+/-}(y)|/|\nabla T|$ are the contributions to the spatially-resolved thermal conductivity along the gradient that stem from the phonons moving in the positive/negative y directions. These two contributions allow us to observe the effect of edge roughness scattering on the position-resolved heat flux across the ribbon. Figure 2 depicts the contributions to the spatially-resolved parallel [Figs. 2(a) and 2(c)] and perpendicular [Figs. 2(b) and 2(d)] thermal conductivity that come from the phonons with wave vectors directed into the top edge (“+”, $q^\perp > 0$) and bottom edge (“−”, $q^\perp < 0$). In the top row [Figs. 2(a) and 2(b)], we see the spatially resolved thermal conductivities of a thin GNR ($W = 15$ nm), while in the bottom row [Figs. 2(c) and 2(d)] the GNR is wide ($W = 1.5$ μm). In general, the parallel and perpendicular components of both κ^+ and κ^- are smallest near the $y = 0$ and $y = W$ edges. The perpendicular mfp $\Lambda_{\text{int}}^\perp$ is an effective width of the region near the edges in which LER significantly affects thermal transport. In wide ribbons, $W \gg 2\Lambda_{\text{int}}^\perp$, $\kappa^{+/-}$ return to their bulk value away from the edges, as shown in Figs. 2(c) and 2(d), so both the parallel and perpendicular thermal conductivities will be close to the “bulk” RTA value (3) throughout most of the GNR. In narrow GNRs ($W > 2\Lambda_{\text{int}}^\perp$), the thermal conductivity is strongly affected by edge scattering and remains well below the bulk RTA value throughout the ribbon [Figs. 2(a) and 2(b)].

However, experiments typically record a spatially averaged thermal conductivity. An effective way to capture the influence

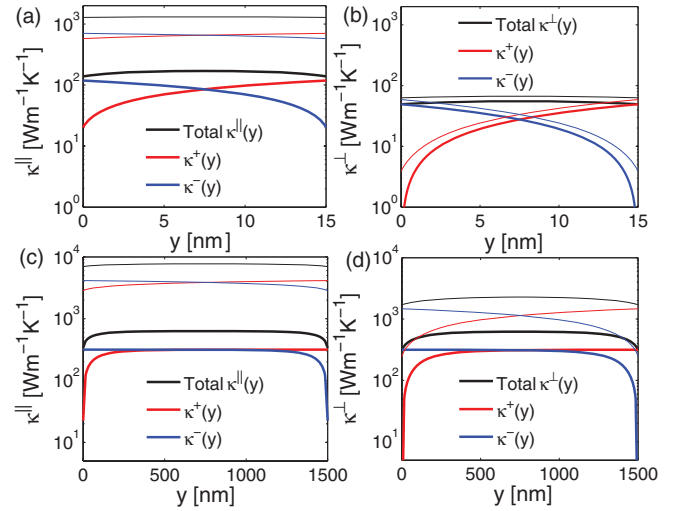


FIG. 2. (Color online) Position dependence of the room-temperature lattice thermal conductivity of graphene nanoribbons in narrow [$W = 15$ nm in (a) and (b)] and wide [$W = 1.5$ μm in (c) and (d)]. Line edge roughness was set to $\Delta = 1$ nm in all cases. The $\kappa^{+/-}$ components, as well as the total thermal conductivities, are plotted in the parallel [panels (a) and (c)] and perpendicular directions [(b) and (d)]. Thick lines are for supported ribbons, where the rapid spatial variation of κ^+ and κ^- is caused by the smaller internal mean free path, limited to 67 nm by the substrate interactions. Thin lines are for suspended ribbons, showing a much slower spatial variation due to the larger internal mean free path, limited only by umklapp phonon-phonon and isotope scattering.

of LER on the transport properties averaged across the GNR would be to introduce an effective LER scattering rate for the entire ribbon. Assuming linear regime and a uniform temperature gradient, an effective phonon-LER scattering rate is obtained by averaging the solution (7) across the ribbon^{20,21}

$$R_{\vec{q}} = \tau_{\text{int}}(\vec{q}) [\tau_{\text{int}}^{-1}(\vec{q}) + \tau_{\text{LER}}^{-1}(\vec{q})] \langle n_{\vec{q}}(y) \rangle. \quad (9)$$

Here, $\langle \dots \rangle$ denotes the spatial average over the y coordinate. Combining Eqs. (3) and (9) and with the pBTE in Eq. (4), we obtain for the LER rate

$$\tau_{\text{LER}}^{-1}(\vec{q}) = \int_0^W v_{\vec{q}}^\perp \frac{\partial n_{\vec{q}}(y)}{\partial y} dy \bigg/ \int_0^W n_{\vec{q}}(y) dy,$$

which is evaluated analytically to obtain the final expression for the LER scattering rate

$$\tau_{\text{LER}}^{-1}(\vec{q}) = \frac{v_{\vec{q}}^\perp}{W} F_p(\vec{q}) \bigg/ \left[1 - \frac{\Lambda_{\text{int}}^\perp(\vec{q})}{W} F_p(\vec{q}) \right]. \quad (10)$$

The competition between line edge roughness scattering and internal scattering mechanisms is encapsulated in the parameter F_p , given by

$$F_p(\vec{q}) = \frac{[1 - p(\vec{q})] \{1 - \exp[-W/\Lambda_{\text{int}}^\perp(\vec{q})]\}}{1 - p(\vec{q}) \exp[-W/\Lambda_{\text{int}}^\perp(\vec{q})]}, \quad (11)$$

which contains the full momentum and angle dependence of line edge roughness scattering through the edge specularly parameter $p(\vec{q})$.

When internal scattering is dominant ($\tau_{\text{int}}^{-1} > \tau_{\text{LER}}^{-1}$, such as in wide ribbons), the two edges become effectively decoupled,

and the rate approaches $\tau_{\text{LER}}^{-1}(\vec{q}) = (v_q^\perp/W)[1 - p(\vec{q})]$. In the opposite limit of narrow ribbons, where LER scattering dominates, the rate converges to the well-known expression²² $\tau_{\text{LER}}^{-1}(\vec{q}) = (v_q^\perp/W)[1 - p(\vec{q})]/[1 + p(\vec{q})]$. Given that $0 \leq p(\vec{q}) \leq 1$, the variation of the LER rate with the strength of competing mechanisms is no larger than a factor of two. However, we note that even when internal scattering is very weak, it cannot be neglected from the derivation because the assumption of no internal scattering ($\tau_{\text{int}}^{-1} = 0$) would lead to an unphysical situation where the solution $n_{\vec{q}}$ is constant and equal everywhere to its value at the edges, implying $N_{\vec{q}}(y) = N_{\vec{q}}^0(T)$ in the limit of completely diffuse ($p = 0$) edges. Such a solution would lead to zero thermal conductivity (or infinite LER scattering rate), which is unphysical and consistent with the lack of the Casimir limit in ribbons.²⁰

The LER scattering rate $\tau_{\text{LER}}^{-1}(\vec{q})$ in Eq. (10) can be added to the substrate, umklapp phonon-phonon, and isotope (mass-difference) scattering that have previously been considered. With the phonon lifetime computed from all the relevant scattering mechanisms, the full thermal conductivity tensor $\mathbf{K}^{\alpha\beta}$ is obtained for the GNR as a sum over all phonon modes and branches^{6,26}

$$\mathbf{K}^{\alpha\beta}(T) = \frac{\hbar}{A\delta} \sum_{b,\vec{q}} v_b^\alpha(\vec{q})v_b^\beta(\vec{q})\tau_b(\vec{q})\omega_b(\vec{q})\frac{dN_{\vec{q}}^0(T)}{dT}, \quad (12)$$

where $\delta = 0.335$ nm is the thickness of the graphene monolayer,¹⁶ $A = LW$ is the area of the ribbon, $\tau_b(\vec{q})$ is the total phonon relaxation time for branch b and mode \vec{q} , and $v_b^\alpha(\vec{q})$ is the α th component of the phonon velocity vector calculated from the full phonon dispersion based on the nearest-neighbor force constant model.^{27,28}

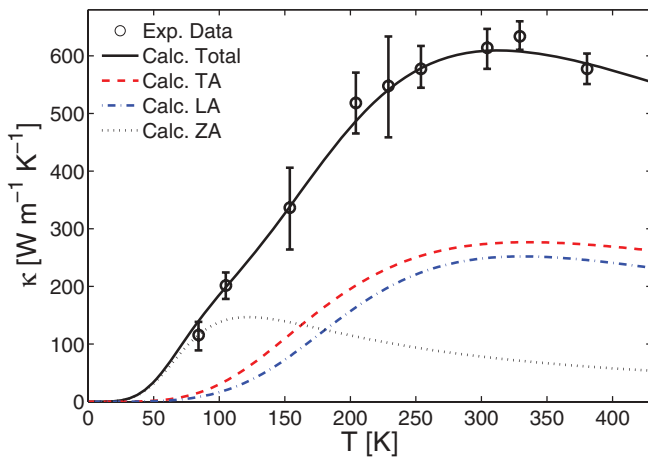


FIG. 3. (Color online) Comparison of lattice thermal conductivity of a wide ($W = 2 \mu\text{m}$) graphene ribbon supported on SiO_2 with experimentally measured data from Ref. 12. Dashed lines are calculated contributions by individual phonon branches and the solid line is the total, showing excellent agreement with experiment throughout the temperature range. At low temperatures, the dominant contribution is from the out-of-plane acoustic (ZA) mode, which gets suppressed by the strong substrate interaction above 100 K, where in-plane modes take over.

III. THERMAL CONDUCTIVITY TENSOR IN SUPPORTED GRAPHENE NANORIBBONS

In Fig. 3, we see that there is excellent agreement between the experimental thermal conductivity data for $2 \mu\text{m}$ -wide GNRs supported on SiO_2 reported in Ref. 12 and the theoretical thermal conductivity computed based on the tensor in Eq. (12). In Fig. 4(a), the effective thermal conductivity of a narrow ribbon ($W = 15$ nm), obtained from the tensor as the average of directional conductivity over all angles (since the experiment entails radial diffusion of heat), reproduces the room temperature mean value of $80 \text{ W m}^{-1} \text{ K}^{-1}$ and the range of measured data reported in Ref. 15. The parallel and perpendicular components of the thermal conductivity tensor differ in these narrow ribbons [Fig. 4(b)]. The $\kappa^{\parallel}/\kappa^{\perp}$ ratio, which captures the anisotropy of thermal transport,

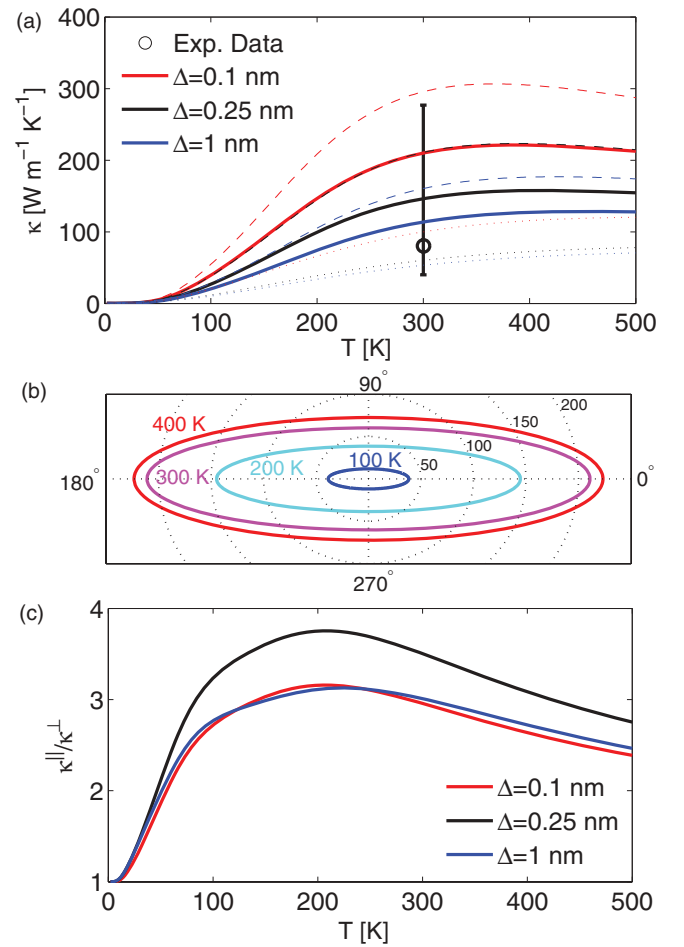


FIG. 4. (Color online) Effective lattice thermal conductivity of a 15-nm-wide graphene nanoribbon supported on a SiO_2 substrate with varying line edge roughness, ranging from 0.1 nm up to 1 nm. The results agree well with the experimental data range reported for that same width of ribbon in Ref. 15. (b) Polar plot of directional thermal conductivity (radial coordinate, in units $\text{W/m}\cdot\text{K}$) versus direction (polar angle with respect to the longitudinal x axis), for temperatures from 100 K to 400 K, in 100 K steps. The spatial anisotropy of thermal conduction can also be depicted through the ratio of the parallel to the perpendicular component of the thermal conductivity tensor in (c). The ratio reaches a value of 3.5 at room temperature in the 15 nm wide ribbon with 0.25 nm edge roughness.

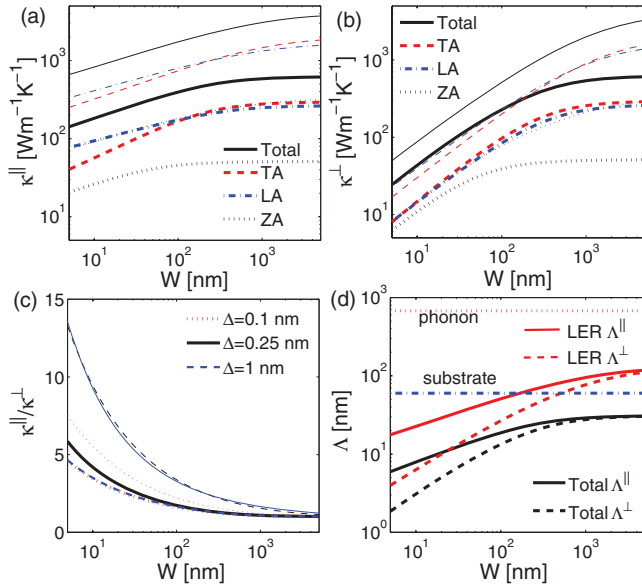


FIG. 5. (Color online) Dependence of the room-temperature parallel (a) and perpendicular (b) lattice thermal conductivities on the width W of supported graphene nanoribbons. Contributions of each acoustic phonon branch, as well as the total, are shown. The longitudinal acoustic (LA) phonons are the least affected by LER scattering and have a dominant contribution to κ^{\parallel} . In contrast, κ^{\perp} shows a steeper dependence on width W , with no clearly dominant branch. The thin lines show the values for the suspended GNR counterparts, demonstrating that the out-of-plane acoustic (ZA) mode is the most suppressed by scattering with the substrate. The $\kappa^{\perp}/\kappa^{\parallel}$ ratio is shown in panel (c) for line edge roughness rms values ranging from $\Delta = 0.1$ nm to $\Delta = 1$ nm. The anisotropy is stronger in narrower ribbons, and ribbons with larger LER values due to the strong dependence [shown in panel (d)] of the parallel and perpendicular components of the LER mfp on width W .

reaches a value of 3.5 just below room temperature in narrow ($W = 15$ nm) ribbons with rms edge roughness of $\Delta = 0.25$ nm, as shown in Fig. 4(c).

As we have seen in Figs. 2(a) and 2(b), for ribbons thinner than $W \approx 2\Lambda_{\text{int.}}^{\perp}$, LER scattering dominates thermal transport. A wider GNR can be divided into three separate regions across: the two regions within a distance $\Lambda_{\text{int.}}^{\perp}$ from either edge, wherein LER scattering dominates, and a region in the middle where internal scattering dominates. As a result, thermal transport in wider wires will be governed by a competition between edge and internal scattering, with decreasing influence of edge scattering as the width increases. Indeed, in Figs. 5(a) and 5(b) we see that the thermal conductivity in both parallel and perpendicular directions increases quickly with increasing ribbon width W up to the point where it reaches $W \approx 2\Lambda_{\text{int.}}^{\perp}$, after which the increase slows down, corresponding to the mix

of internal and LER scattering. Both thermal conductivities eventually saturate at the bulk value for widths of order micron.

In supported ribbons, the dominant internal scattering mechanism is substrate scattering. We calculated the room-temperature phonon mfp [Fig. 5(d)], due to substrate interactions from Eq. (2) to be 67 nm, an order of magnitude smaller than the umklapp-limited value of the mfp in suspended graphene (677 nm^{6,16}), which agrees with the drastic reduction of thermal conductivity even in wide ($W \approx 2 \mu\text{m}$), supported ribbons (Ref. 12). Substrate scattering is spatially isotropic because it depends only on the magnitude of the phonon momentum. Consequently, the thermal conductivity tensor in wide ribbons is nearly isotropic [Fig. 5(c)], making them good omnidirectional heat spreaders. In contrast, heat flow in narrow ribbons is dominated by the edge regions, where strong anisotropy arises out of LER scattering and makes them better suited as directional (longitudinal) conduits of heat.

IV. CONCLUSION

In summary, we have calculated the full thermal conductivity tensor in supported graphene nanoribbons on SiO₂. We show that thermal transport in GNRs is characterized by a complex interplay between LER scattering and internal scattering, as captured through an effective LER scattering rate that depends not only on the surface roughness features, but also on the strength of internal scattering mechanisms (substrate, isotope, and umklapp phonon scattering). In suspended GNRs, internal scattering mechanisms are fairly weak (the room-temperature mfp 677 nm), so this interplay is difficult to observe; rather, LER scattering dominates and thermal transport is spatially anisotropic for virtually any suspended GNR width. In contrast, internal scattering in supported GNRs is dominated by the substrate interactions and the mfp is an order of magnitude shorter (≈ 67 nm). As a result, thermal transport features acquire a more prominent width dependence: lattice thermal conductivity in narrow supported GNRs ($W < 130$ nm, i.e., twice the mfp for substrate scattering) is dominated by LER scattering and strongly spatially anisotropic. For intermediate widths ($130 \text{ nm} < W < 1 \mu\text{m}$) a competition between LER and substrate scattering governs transport, while the thermal transport in wide GNRs ($W > 1 \mu\text{m}$) is dominated by substrate scattering and spatially isotropic.

ACKNOWLEDGMENTS

This work has been supported by the Computing Innovation Fellows Project (NSF Grant No. 0937060 to the Computing Research Association, sub-award CIF-146 to the University of Wisconsin), by the NSF (Grant Nos. ECCS-1201311 and OCI-1122690), and by the AFOSR YIP program (Grant No. FA9550-09-1-0230).

*aksamija@wisc.edu

†knezevic@engr.wisc.edu

¹A. A. Balandin, S. Ghosh, W. Bao, I. Calizo, D. Teweldebrhan, F. Miao, and C. N. Lau, *Nano Lett.* **8**, 902 (2008).

²S. Ghosh, I. Calizo, D. Teweldebrhan, E. P. Pokatilov, D. L. Nika, A. A. Balandin, W. Bao, F. Miao, and C. N. Lau, *Appl. Phys. Lett.* **92**, 151911 (2008).

³A. A. Balandin, *Nat. Mater.* **10**, 569 (2011).

- ⁴P. Klemens and D. Pedraza, *Carbon* **32**, 735 (1994).
- ⁵B. D. Kong, S. Paul, M. B. Nardelli, and K. W. Kim, *Phys. Rev. B* **80**, 033406 (2009).
- ⁶D. L. Nika, E. P. Pokatilov, A. S. Askerov, and A. A. Balandin, *Phys. Rev. B* **79**, 155413 (2009); D. L. Nika, S. Ghosh, E. P. Pokatilov, and A. A. Balandin, *Appl. Phys. Lett.* **94**, 203103 (2009).
- ⁷J. Lan, J.-S. Wang, C. K. Gan, and S. K. Chin, *Phys. Rev. B* **79**, 115401 (2009).
- ⁸A. V. Savin, Y. S. Kivshar, and B. Hu, *Phys. Rev. B* **82**, 195422 (2010).
- ⁹W. J. Evans, L. Hu, and P. Keblinski, *Appl. Phys. Lett.* **96**, 203112 (2010).
- ¹⁰E. Munoz, J. Lu, and B. I. Yakobson, *Nano Lett.* **10**, 1652 (2010).
- ¹¹M. Freitag, M. Steiner, Y. Martin, V. Perebeinos, Z. Chen, J. C. Tsang, and P. Avouris, *Nano Lett.* **9**, 1883 (2009).
- ¹²J. H. Seol, I. Jo, A. L. Moore, L. Lindsay, Z. H. Aitken, M. T. Pettes, X. Li, Z. Yao, R. Huang, D. Broido, N. Mingo, R. S. Ruoff, and L. Shi, *Science* **328**, 213 (2010).
- ¹³J.-H. Chen, C. Jang, S. Xiao, M. Ishigami, and M. S. Fuhrer, *Nature Nano.* **3**, 206 (2008).
- ¹⁴T. Fang, A. Konar, H. Xing, and D. Jena, *Phys. Rev. B* **78**, 205403 (2008).
- ¹⁵A. D. Liao, J. Z. Wu, X. Wang, K. Tahy, D. Jena, H. Dai, and E. Pop, *Phys. Rev. Lett.* **106**, 256801 (2011).
- ¹⁶Z. Aksamija and I. Knezevic, *Appl. Phys. Lett.* **98**, 141919 (2011).
- ¹⁷Y. Xu, X. Chen, B.-L. Gu, and W. Duan, *Appl. Phys. Lett.* **95**, 233116 (2009).
- ¹⁸J.-W. Jiang, J.-S. Wang, and B. Li, *Phys. Rev. B* **79**, 205418 (2009).
- ¹⁹K. Saito, J. Nakamura, and A. Natori, *Phys. Rev. B* **76**, 115409 (2007).
- ²⁰Z. Wang and N. Mingo, *Appl. Phys. Lett.* **99**, 101903 (2011).
- ²¹P. Carruthers, *Rev. Mod. Phys.* **33**, 92 (1961).
- ²²J. Ziman, *Electrons and Phonons: The Theory of Transport Phenomena in Solids* (Oxford University Press Inc., New York, 1960).
- ²³S. B. Soffer, *J. Appl. Phys.* **38**, 1710 (1967).
- ²⁴Z. Aksamija and I. Knezevic, *Phys. Rev. B* **82**, 045319 (2010).
- ²⁵Z. Aksamija and I. Knezevic (unpublished).
- ²⁶S. Ghosh, D. L. Nika, E. P. Pokatilov, and A. A. Balandin, *New J. Phys.* **11**, 095012 (2009).
- ²⁷R. Saito, G. Dresselhaus, and M. S. Dresselhaus, *Physical Properties of Carbon Nanotubes* (Imperial College Press, London, 1998).
- ²⁸J. Zimmermann, P. Pavone, and G. Cuniberti, *Phys. Rev. B* **78**, 045410 (2008).